Title

Nanoparticle-modified microrobots for in vivo antibiotic delivery to treat acute bacterial pneumonia

Journal

Nature Materials, 21(11)

ISSN

1476-1122

Authors

Zhang, Fangyu
Zhuang, Jia
Li, Zhengxing
et al.

Publication Date

2022-11-01

DOI

10.1038/s41563-022-01360-9

Peer reviewed

HHS Public Access

Author manuscript

Nat Mater. Author manuscript; available in PMC 2023 May 01.

Published in final edited form as:

Nat Mater. 2022 November ; 21(11): 1324–1332. doi:10.1038/s41563-022-01360-9.

Nanoparticle-modified microrobots for in vivo antibiotic delivery to treat acute bacterial pneumonia

Fangyu Zhang[1,†], **Jia Zhuang**[1,†], **Zhengxing Li**[1,†], **Hua Gong**[1,†], **Berta Esteban-Fernández de Ávila**[1], **Yaou Duan**[1], **Qiangzhe Zhang**[1], **Jiarong Zhou**[1], **Lu Yin**[1], **Emil Karshalev**[1], **Weiwei Gao**[1], **Victor Nizet**[2], **Ronnie H. Fang**[1], **Liangfang Zhang**[1,*], **Joseph Wang**[1,*]

[1]Department of NanoEngineering and Chemical Engineering Program, University of California San Diego, La Jolla, CA 92093, United States.

[2]Department of Pediatrics and Skaggs School of Pharmacy and Pharmaceutical Sciences, University of California San Diego, La Jolla, CA 92093, United States.

Abstract

Bioinspired microrobots capable of actively moving in biological fluids have attracted considerable attention for biomedical applications because of their unique dynamic features that are otherwise difficult to achieve by their static counterparts. Here, we use click chemistry to attach antibiotic-loaded neutrophil membrane-coated polymeric nanoparticles to natural microalgae, thus creating hybrid microrobots for the active delivery of antibiotics in the lungs *in vivo*. The microrobots show fast speed (> 110 μm s^{-1}) in simulated lung fluid and uniform distribution into deep lung tissues, low clearance by alveolar macrophages, and superb tissue retention time (> 2 d) after intratracheal administration to test animals. In a mouse model of acute *Pseudomonas aeruginosa* pneumonia, the microrobots effectively reduce bacterial burden and substantially lessen animal mortality, with negligible toxicity. Overall, these findings highlight the attractive functions of the algae-nanoparticle hybrid microrobots for active *in vivo* delivery of therapeutics to the lungs in intensive care unit settings.

Editor summary:

Biohybrid microrobots consisting of nanoparticle-modified microalgae are constructedfor active drug delivery in the lungs. In an acute bacterial pneumonia model, the microrobotseffectively reduce bacterial burden and lessen animal mortality.

The potential of micro/nanorobots for biomedical applications has been explored extensively over the last decade[1–3]. While early microrobot designs, consisting primarily of rigid metallic or polymeric structures, allowed for various *in vitro* applications, novel platforms

* josephwang@ucsd.edu; zhang@ucsd.edu.

† These authors contributed equally to this work.

Author contributions

F.Z., Jia.Z., L.Z. and J.W. conceived the study and designed experiments. F.Z., Jia.Z., Z.L. and H.G. conducted the experiments. F.Z., Jia.Z., Z.L., H.G., B.E., Y.D., Q.Z., Jiar.Z., L.Y., E.K., R.F., L.Z. and J.W analyzed the data. F.Z., Jia.Z., Z.L., H.G., B.E., W.G., V.N., R.F., L.Z. and J.W wrote the manuscript. All the authors reviewed, edited, and approved the paper.

Competing interests

The authors declare no competing interests.

based on biocompatible and deformable materials have offered some unique advantages towards *in vivo* operations, including improved drug delivery, deep tissue imaging, and precision microsurgery[4–6]. The *in vivo* application of these microrobots has typically been restricted due to limitations in availability of natural fuels, accessibility to certain organs and tissues, and potential toxicity. Biodegradable zinc and magnesium-based microrobots have been used for drug delivery in the gastrointestinal (GI) tract[7,8]. Magnetically powered microrobots have demonstrated deep penetration in the vitreous humor[6] and actuation in the peritoneal cavity[9,10]. Achieving active propulsion in other body locations is difficult, but if successful, would offer unprecedented benefits for the treatment of important diseases.

Herein, we report on a bioinspired microrobot platform consisting of nanoparticle-modified algae for active therapeutic delivery to treat lung disease. Biohybrid microrobots, which combine the motility of natural organisms with the multifunctionality of synthetic components, have recently been studied as an alternative to purely synthetic microrobots[11,12]. For instance, *Magnetococcus marinus*, which swim along local magnetic fields and toward low oxygen concentrations, were used for transporting drugs into hypoxic tumor regions[13]. The natural movement of sperm has been leveraged to construct hybrid microrobots with distinct advantages toward assisted fertilization[14]. In our design, we create a biohybrid microrobot consisting of *Chlamydomonas reinhardtii* microalgae modified with neutrophil membrane-coated and drug-loaded polymeric nanoparticles (denoted ‘algae-NP-robot’) for *in vivo* treatment of lung infection (Fig. 1a). *C. reinhardtii*-based microswimmers have been used recently as microcarriers of synthetic cargos, demonstrating efficient movement and biocompatibility[15,16]. They can be facilely cultured and offer self-propulsion based on flagella beating ($\geq 110\ \mu m\ s^{-1}$), intrinsic autofluorescence, phototactic guidance, and a long lifespan[17]. The neutrophil membrane-coated nanoparticles are used because of their unique cell-mimicking properties, including shielding payloads from biological environments, reducing immune clearance, and enabling specific binding with target pathogens[18]. The unique properties of natural algae are combined with the engineering versatility of biomimetic nanoparticles to yield a hybrid microrobot platform capable of active drug delivery.

Among the numerous applicable conditions, we choose to first test the algae-NP-robot for *in vivo* antibiotic delivery to treat bacterial lung infections. Specifically, ventilator-associated pneumonia (VAP) is an acute and potentially fatal infection characterized by onset 48 hours after initiation of mechanical ventilation in intensive care unit (ICU) settings[19]. VAP represents one of the most common infections among hospital patients, affecting between 10–25% of those who are intubated[20], resulting in significant mortality, prolonged ICU stays, and an increased number of days on ventilation[21–23]. Multidrug-resistant pathogens such as *Pseudomonas aeruginosa* are becoming increasingly prevalent as antibiotics continue to be used indiscriminately and with waning effectiveness[24]. We hypothesized that pulmonary antibiotic delivery efficiency could benefit from the deep tissue penetration and prolonged drug retention enabled by the algae-NP-robot system in an experimental model of VAP.

To transform microalgae into algae-NP-robot, we first modified the algal surface with azido N-hydroxysuccinimide (NHS) ester[25,26], followed by conjugation with dibenzocyclooctyne

(DBCO)-modified neutrophil membrane-coated polymeric nanoparticles via click chemistry (Fig. 1b). This type of reaction has been used to modify cells for a number of applications[27–29]. The motion and cargo-carrying behavior of the resulting algae-NP-robot in simulated lung fluid (SLF), combined with their uniform distribution, effective inhibition of macrophage phagocytosis, and prolonged retention in lung tissue, is verified and highlights the considerable promise of the platform for *in vivo* drug delivery. Additionally, the therapeutic efficacy and safety of the drug-loaded algae-NP-robot are demonstrated using a murine model of *P. aeruginosa* lung infection.

Preparation of algae-NP-robot

C. *reinhardtii* algae were cultivated in tris-acetate-phosphate (TAP) medium (Supplementary Fig. 1). For further modification, the algae were conjugated with azido-PEG_4-NHS ester, which reacts with primary amines on the algal surface. The algae functionalization was confirmed, and negligible cytotoxicity was observed (Supplementary Fig. 2). We then fabricated neutrophil membrane-coated poly(lactic-*co*-glycolic acid) (PLGA) nanoparticles[30] (denoted 'NPs') for use as the therapeutic payload. For visualization, the hydrophobic dyes 1,1'-dioctadecyl-3,3,3',3'-tetramethylindocarbocyanine perchlorate (DiI) and 3,3'-dioctadecyloxacarbocyanine perchlorate (DiO) were loaded into the PLGA cores and the neutrophil membrane, respectively. The overlap of both fluorescence signals indicated the successful association of the two components (Fig. 1c). The NPs were further characterized by dynamic light scattering, transmission electron microscopy (TEM), and immunostaining, verifying their core–shell structure and right-side-out membrane orientation (Supplementary Fig. 3). The surface of the NPs was further reacted with DBCO-PEG_4-NHS ester, and successful modification was confirmed qualitatively by fluorescence microscopy using an azide-functionalized dye (Supplementary Fig. 4). Conjugation to the algal surface was achieved through click chemistry by incubating the azido-modified algae with the DBCO-modified NPs. Scanning electron microscopy (SEM) imaging confirmed the formation of NP-modified algae (Fig. 1d, Supplementary Fig. 5a,b). By optimizing the NP input concentration, 91.2% of the algae population could be conjugated with NPs (Fig. 1e, Supplementary Fig. 5c). Fluorescence microscopy was used to confirm that the NPs were firmly attached to the algal surface after multiple washing steps (Fig. 1f,g).

Motion behavior of algae-NP-robot

The speed of algae-NP-robot (104.6 ± 11.2 μm s^{-1}) was similar to that of the bare algae (115.5 ± 11.8 μm s^{-1}) in TAP medium at 22 °C (Supplementary Fig. 6a), suggesting that NP coupling had a negligible effect on algae motility. As we sought to leverage algae-NP-robot for deep lung delivery, propulsion characteristics in simulated lung fluid (SLF)[31] were first evaluated (Supplementary Table 1). The motion behavior of bare algae at room temperature (RT, 22 °C) and at body temperature (BT, 37 °C) in SLF was compared (Fig. 2a–c and Supplementary Movie 1). The bare algae maintained a steady speed of ~115 μm s^{-1} (11.5 body lengths per second) over 1 h at RT but displayed a gradual decrease in speed from ~101 μm s^{-1} to ~55 μm s^{-1} at BT, indicating that higher temperatures could impact algae motion[32]. The growth rate of bare algae was monitored at both temperatures, and inhibition of growth was observed at BT[33] (Supplementary Fig. 6b). Algae-NP-robot demonstrated

similar trends in their motion (Fig. 2d–f). To mimic the elevated body temperature of patients with VAP, an additional test was carried out at 40 °C, and no significant differences were observed compared with algae-NP-robot at BT. Fig. 2g–l show representative tracking trajectories of individual algae-NP-robot over 0, 1, and 2 s intervals (Supplementary Movie 2) and the corresponding mean speed distribution in SLF at different operation times at BT. It is important to note that 95% of the algae remained viable after 1 h of motion in SLF, reflecting the good adaptivity of algae under these conditions (Supplementary Fig. 6c,d). At longer timepoints of 12 h and 24 h, approximately 85% and 60% of the algae-NP-robot, respectively, remained motile when exposed to SLF in the dark at BT; this percentage further decreased to less than 20% after 48 h of exposure (Supplementary Fig. 6e and Movie 4). Algae-NP-robot did not exert cytotoxicity when incubated with different cell types (Supplementary Fig. 7), and their capacity for phototaxis was unaffected (Supplementary Fig. 8 and Movie 5). Overall, these results demonstrate that modification with NPs has a negligible effect on the intrinsic motion behavior of algae, allowing algae-NP-robot to be employed as an active delivery platform in physiological conditions.

In vivo distribution, retention, and clearance in the lungs

The lung distribution of algae-NP-robot was examined after intratracheal administration[34]. Leveraging the autofluorescence from the algae's chloroplasts, the distribution was visualized by *ex vivo* fluorescence imaging of excised lungs at various timepoints (Fig. 3a). Fluorescence from the algae-NP-robot permeated throughout the lung tissue within 1 h, and the strong signal was retained for at least 24 h. In contrast, NP-modified deflagellated algae (denoted 'static algae-NP'), incapable of moving, was characterized by SEM and used as a control (Supplementary Fig. 9). The signal of static algae-NP decreased sharply within 4 h and nearly disappeared after 12 h, highlighting the role of active motion in promoting robust lung distribution and retention. To quantitatively compare the algae retention, we homogenized the lungs and measured the fluorescence intensity. The total fluorescence of the algae-NP-robot decreased slowly over the course of 72 h and was significantly higher than that of the static algae-NP up to 48 h. After 72 h, the fluorescence intensity returned to near baseline for both groups (Supplementary Fig. 10). Normalized fluorescence data further verified the slower clearance of algae-NP-robot, as 86% and 65% of the original signal were present at 4 h and 24 h, respectively (Fig. 3b). In comparison, static algae-NP exhibited greatly reduced signals, with 24% and 8% remaining at 4 h and 12 h, respectively. Overall, these data indicate that the motion behavior of algae-NP-robot greatly improved their lung retention.

To better understand the greatly reduced clearance of algae-NP-robot compared with static algae-NP, we sought to elucidate the potential role of macrophages, an abundant cell population in the lung alveoli capable of clearing exogenous species by phagocytosis[35]. Algae-NP-robot and static algae-NP were mixed with murine J774 macrophages at a 1:1 ratio and incubated at 37 °C in the dark. Fig. 3c displays the different stages of the algae-NP-robot phagocytosis by macrophages. Algae-NP-robot showed strong autofluorescence from the algae before binding and upon contacting the macrophage (0 min). After being taken up by the macrophages via phagocytosis, the algae-NP-robot was gradually degraded, as indicated by a progressive decrease in autofluorescence (15 min to 75 min). By

counting the numbers of unbound algae-NP-robot and macrophages at different timepoints (Supplementary Fig. 11a), the uptake of algae-NP-robot over time was quantified. As shown in Fig. 3d, static algae-NP were internalized significantly faster than their active counterparts, indicating that active motion facilitates escape from macrophage uptake (Supplementary Movie 3). A cryo-treated algae-NP-robot, incapable of moving, was also taken up faster by macrophages compared to algae-NP-robot, confirming that the physical presence of flagella is not a major factor in the inhibition of phagocytosis (Supplementary Fig. 11b). Quantification of the total fluorescence intensity showed that the signal of the algae-NP-robot was consistently higher than that of the static control during 72 h of incubation (Supplementary Fig. 12a). Compared to the uptake profiles in Fig. 3d, the relative fluorescence profiles of the algae were reversed (Fig. 3e). It should be noted that the optical absorbance and fluorescence of the algae-NP-robot without the macrophages was constant (Supplementary Fig. 12b,c), further supporting that macrophage phagocytosis was an important reason for the observed lung clearance kinetics.

To better understand the clearance mechanism *in vivo*, flow cytometry analysis of the macrophage uptake was performed at different timepoints after intratracheal administration in mice (Fig. 3f,g and Supplementary Fig. 13). Minimal uptake of algae-NP-robot by alveolar macrophages was observed within the first 12 h, and a large increase of uptake was observed at 48 h. In comparison, approximately 20% of the macrophages were positive for static algae-NP uptake after only 1 h, with the uptake peaking at 4 h post-administration before decreasing at later timepoints. The decreased signal is attributed to the degradation of algae after uptake, which destroys their autofluorescence as observed in Fig. 3c. These results indicate that alveolar macrophage uptake is a major clearance mechanism for algae in the lungs. The delayed *in vivo* uptake of the algae-NP-robot by alveolar macrophages corroborates the *in vitro* findings and could explain the enhanced lung retention that was observed.

Drug loading and *in vivo* antibacterial efficacy

Based upon the uniform lung distribution and prolonged retention, we postulated that algae-NP-robot may serve as an effective drug carrier for treating infection in the lower respiratory tract. In the study, ciprofloxacin (Cip), a common antibiotic drug used in combinational regimens against susceptible strains of *P. aeruginosa*, was encapsulated into NP (denoted ‘NP(Cip)’). The drug loading was optimized to meet the therapeutic threshold for *P. aeruginosa*[36]. The same method as before was used to fabricate algae conjugated with the drug-loaded NPs (denoted ‘algae-NP(Cip)-robot’). We then evaluated the Cip loading yield onto the algae (Fig. 4a). Using a constant drug input, the total amount of Cip loaded increased linearly with algae number up to approximately 4×10^7 algae and then slowly saturated. The formulation consisting of 6 μg Cip loaded onto 4×10^7 algae was thus selected for subsequent *in vitro* and *in vivo* studies. Similar to NP(Cip), algae-NP(Cip)-robot demonstrated an initial burst release of drug over the initial 20 h, followed by a slow release up to 96% by 72 h (Fig. 4b). The minimal inhibitory concentration (MIC) against *P. aeruginosa* was then evaluated (Supplementary Fig. 14). Bacterial growth was inhibited at a Cip concentration of 62.5 ng ml^{-1} for all groups (Fig. 4c), consistent with what has been previously reported[37]. Fig. 4d shows the enumerated bacterial colony forming units (CFU)

after treatment with algae-NP(Cip)-robot and with other controls, enabling us to establish the minimal bactericidal concentration (MBC). Algae-NP(Cip)-robot had a comparable inhibitory efficacy to free Cip, and the MBC of both was determined to be 125 ng ml^{-1}. Bare algae and NPs had negligible effects on the bacteria, supporting that the inhibitory efficacy of algae-NP(Cip)-robot was due solely to the loaded Cip (Supplementary Fig. 15). An *in vitro* study was also performed to confirm that the algae-NP-robot is able to bind to *P. aeruginosa*. After 24 hours of incubation, signal from the Hoechst 33342-stained DNA of the bacteria colocalized with that of the DiI-labeled NPs, demonstrating effective binding between the two (Supplementary Fig. 16a). The binding efficiency was further quantified by enumeration of unbound bacteria, revealing that 95% of the initial bacterial input was bound to algae-NP-robot (Supplementary Fig. 16b). Such binding is thought to be mediated by protein receptors present on the surface of the NPs[38]. To further verify the unique binding properties of the NPs, PLGA nanoparticle cores without membrane coating and liposomes were used, and neither control bound effectively to the bacteria (Supplementary Fig. 17).

Next, we examined the ability of algae-NP(Cip)-robot to treat acute lung infection *in vivo*. *P. aeruginosa* was first inoculated to characterize bacterial dispersion within the lungs (Supplementary Fig. 18). The data demonstrated that the bacteria disseminated throughout the entirety of lungs within 1 h after intratracheal inoculation, suggesting that algae-NP-robot could be used to efficiently treat conditions like VAP. To investigate antibacterial efficacy against *P. aeruginosa* pneumonia, algae-NP(Cip)-robot or control samples were intratracheally administered 30 min after bacterial inoculation. An antibiotic dose of 500 ng Cip was administered per mouse (Supplementary Fig. 19). The lungs were then collected, followed by homogenization for bacterial enumeration 24 h after administration. As illustrated in Fig. 4e, the bacterial burden after the algae-NP(Cip)-robot treatment was quantified as 2.6×10^4 CFU g^{-1}, representing a 3 orders of magnitude reduction compared with the negative control (2.6×10^7 CFU g^{-1}), and a significant reduction compared with static algae-NP(Cip) (6.5×10^5 CFU g^{-1}) and NP(Cip) (3.8×10^5 CFU g^{-1}). A survival study was conducted using the same experimental setup (Fig. 4f). Algae-NP(Cip)-robot treatment of infected mice resulted in 100% survival over the entire duration of the 30-day study ($p < 0.0001$, n = 12). In stark contrast, all untreated mice died within 3 days. Survival rates of mice treated with NP(Cip) or static algae-NP(Cip) were 25% and 16.7%, respectively. We concluded that the prolonged lung retention and sustained release characteristics of algae-NP(Cip)-robot enabled the significant improvement in survival compared to the control groups. Subsequently, we compared the efficacy of algae-NP(Cip)-robot with the conventional treatment of intravenous (IV) Cip. The algae-NP(Cip)-robot treatment significantly outperformed IV Cip at the same drug dosage (500 ng per mouse) and achieved similar efficacy compared with IV Cip at a more clinically relevant dosage (1.644 mg per mouse). Additional experiments were performed to quantify the lung bacterial burden at later timepoints following algae-NP(Cip)-robot treatment, revealing a progressive decrease over time and complete clearance after 1 week (Fig. 4g). To verify the effectiveness of algae-NP(Cip)-robot with delayed treatment, we performed an additional study in which mice were treated at progressively longer intervals after a lethal *P. aeruginosa* challenge (Fig. 4h,i). While the therapeutic efficacy decreased as the treatment interval increased, a significant reduction was still observed even with a 6 h delay.

Biosafety evaluation

Lastly, to verify the biosafety of algae-NP(Cip)-robot, a comprehensive analysis of blood chemistry and major blood cell populations was conducted 24 h, 72 h, and 168 h after administration into the lungs (Fig. 5a,b). Compared to mice administered with TAP buffer only, little difference was observed for all the blood parameters. The heart, liver, spleen, lungs, and kidneys were also processed by hematoxylin and eosin (H&E) staining (Fig. 5c–e). The overall structural integrity of all tissues was nearly identical to those from mice administered with TAP buffer, demonstrating no signs of acute toxicity and further supporting the safety of algae-NP(Cip)-robot. To further evaluate for potential inflammatory responses in the lungs, different cytokines (TNF-α, IL-1β, and IL-6) were analyzed 24 h, 72 h, and 168 h after intratracheal administration of the algae-NP(Cip)-robot into the lungs. No significant difference in cytokine levels was observed for the algae-NP(Cip)-robot treatment compared to the control group (Fig. 5f–h). Histological sections of lung tissues collected over time at 24 h, 72 h, and 168 h after administration revealed negligible leukocyte infiltration, normal structures of the lung tissue, and no signs of inflammation (Fig. 5i). Further *in vitro* studies verified that algae-NP-robot, in contrast to bacterial flagellin[39], did not trigger the significant production of proinflammatory cytokines by innate immune cells (Supplementary Fig. 20). Together, these data suggest the favorable safety profile of the algae-NP-robot delivery platform.

Outlook

The biohybrid microrobot platform described in this work creates new opportunities for active drug delivery to the lungs of ventilated ICU patients. This is due to its distinct advantages in terms of facile large-scale production, autonomous motion and long lifespan in localized environments, intrinsic autofluorescence for easy *in vivo* observation, and potential targeting functionality. Further studies are required to determine if our biohybrid microrobot system can deliver key antibiotics for treating other important bacterial pathogens in VAP, including *Acinetobacter baumannii* and *Staphylococcus aureus*, or be extended to treatment of other ICU conditions such as acute respiratory distress syndrome (ARDS) that is a complication of viral pneumonia. Future studies will also test the algae-NP-robot formulation against clinical *P. aeruginosa* isolates to evaluate its general applicability. In its current iteration for intratracheal administration, the biohybrid microrobot would not be suitable for treating chronic *P. aeruginosa* infections, such as those that afflict the lungs of cystic fibrosis patients, or for other patients in which mechanical ventilation or bronchoscopy is not indicated by their clinical status. Prior to human clinical trials, additional validation using large animal models suitable for repeated dosing studies would enable better evaluation of algae-NP-robot therapeutic efficacy and safety in comparison to clinical IV antibiotic regimens. Looking forward, it would also be interesting to more precisely understand how algae-based microrobots interact with the immune system, aiming to further improve their retention time in the lungs. Exploring different delivery methods, such as by inhalation or intravenous administration, or leveraging the inherent phototaxis properties of algae, may expand the scope of the platform across a wider range of applications.

While the treatment of acute pneumonia using algae-NP-robot likely benefited from uniform dispersion throughout the lungs, biohybrid microrobots can also be integrated with sensory and targeting functionalities for situations in which more precise delivery is required. For example, optogenetics technology that locally induces the light emission of target cells with photoreceptors[40] can be introduced to trigger the inherent phototaxis of algae[41], thus enabling site-specific targeting[42]. The algae can also be genetically engineered with functional proteins on their surface to introduce additional functionalities[43]. Besides algae, other microorganisms with specific sensory or targeting capabilities[13,44] could also be used in the development of autonomous drug delivery vehicles for treating pulmonary diseases.

Methods

Algae culture.

Green *C. reinhardtii* algae (strain CC-125 wild-type mt+) were obtained from the Chlamydomonas Resource Center. The algae were transferred from the agar plate to Tris-acetate-phosphate (TAP) medium (Thermo Fisher Scientific) and cultivated at room temperature under cycles of 12 h sunlight and 12 h dark.

Neutrophil cell culture.

Human neutrophil-like cells (HL-60, American Type Culture Collection, ATCC CCL-240) were cultured in RPMI 1640 (11875135, Gibco) with 1 v/v% penicillin-streptomycin (15140122, Gibco) and 10 v/v% fetal bovine serum (SH30541.03, Hyclone) in an incubator under 5% CO_2 at a temperature of 37 °C. Cells were regularly tested for mycoplasma.

Neutrophil cell membrane derivation.

HL-60 plasma membrane was collected according to an established procedure[23]. Frozen cells were thawed and washed 3 times with 1× PBS. Cells were lysed in a buffer consisting of 30 mM Tris-HCl, 75 mM sucrose, 225 mM D-mannitol, 0.2 mM ethylene glycol-bis(β-aminoethyl ether)-N,N,N’,N’-tetraacetic acid, and phosphatase/protease inhibitor mixtures (Sigma Aldrich). Cells were next homogenized using a Kinematica Polytron PT-10/35 probe homogenizer, and the cell membrane was collected through gradient centrifugation. BCA kit (Pierce) was used to quantify the cell membrane content. The final cell membrane was stored in 0.2 mM EDTA at −80 °C for subsequent studies.

Synthesis of polymeric cores.

Drug loaded polymeric cores were synthetized following a reported method with slight modifications[45]. Briefly, 50 μl of 25 mg ml^{-1} ciprofloxacin (HCl salt, Sigma Aldrich) solution was emulsified in 500 μl chloroform solution containing 50 mg ml^{-1} poly(lactic-*co*-glycolic acid) (50:50 PLGA, 0.67 dl g^{-1}, Lactel Absorbable Polymers) using an ultrasonic probe sonicator (Fisher Scientific) operating at a power of 10 W. The sonication lasted for 2 min with alternating cycles of 2 s power on and 2 s power off inside an ice bath. Then, the emulsion was transferred to 10 ml of aqueous solution and sonicated for another 2 min. The emulsion was stirred for 4 h to completely evaporate the chloroform. All samples were centrifuged for 5 min at 16,100*g* and washed twice with ultrapure water, and lyophilized for future use. The 3,3’-dioctadecyloxacarbocyanine perchlorate (DiO, $\lambda_{ex}/\lambda_{em}$

= 484 nm/501 nm; Thermo Fisher Scientific)-loaded nanoparticles were synthesized by replacing ciprofloxacin with 1 mg ml^{-1} of the dye and then following the same method.

Synthesis of neutrophil membrane-coated nanoparticles.

Neutrophil membrane-coated nanoparticles were synthesized by an established procedure[18]. Briefly, the neutrophil membranes were added into solution containing PLGA cores at a polymer to membrane protein weight ratio 1:1. The neutrophil membranes were coated onto PLGA cores through 3 min sonication in a bath sonicator (Fisher Scientific FS30D). The resulting membrane-coated nanoparticles were separated from the solution by 5 min centrifugation at 16,100*g* and washed twice with ultrapure water.

Characterization of neutrophil membrane-coated nanoparticles.

The nanoparticle size and surface charge of neutrophil membrane-coated nanoparticles were measured using dynamic light scattering (ZEN 3600 Zetasizer, Malvern). In addition, the morphology of nanoparticles was verified using transmission electron spectroscopy (FEI 200 kV Sphera). Brightfield and fluorescent images of 1,1'-dioctadecyl-3,3,3',3'-tetramethylindocarbocyanine perchlorate (DiI, $\lambda_{ex}/\lambda_{em}$ = 551 nm/566 nm; Thermo Fisher Scientific)-labeled neutrophil membrane and DiO-loaded PLGA core were taken on a fluorescence microscopy (EVOS FL). To verify the neutrophil membrane orientation after coating, neutrophils (~2.5×10^6 cells) and neutrophil membrane-coated nanoparticles (100 μl, 0.5 mg ml^{-1} protein content) were blocked in 1% bovine serum albumin (BSA, Millipore Sigma) for 30 min and then incubated with 1 μl 100 mg ml^{-1} Alexa488 anti-human CD11a (LFA-1) antibody (Biolegend) for 30 min. The total fluorescent intensity of the mixture was measured by BioTek Synergy Mx microplate reader. To separate unbound antibodies, neutrophil samples were spun down at 3000*g* for 5 min, whereas neutrophil membrane-coated nanoparticles were centrifuged for 5 min in 300 kDa molecular weight cutoff Nanosep tubes at 5000*g*. The fluorescence intensity of the unbound antibodies was measured in order to determine the amounts bound to the neutrophils and NPs.

Preparation of algae-NP-robot.

Green algae were washed with ultrapure water three times to remove any residual TAP buffer, and they were subsequently resuspended in ultrapure water. Then, 1×10^7 algae were treated with 20 μM azido-PEG_4-NHS ester (Click Chemistry Tools) for 45 min at room temperature. To examine the effective binding of azido groups on the algae surface, the resulting algae were incubated with BDP FL DBCO (Lumiprobe) for 30 min and then subjected to flow cytometry analysis (1×10^4 events were collected for analysis). Then neutrophil membrane-coated PLGA nanoparticles (denoted 'NP') were modified with N_3 bonds for the click chemistry. Here, NP were incubated with 40 μM DBCO-PEG_4-NHS ester for 1 h at room temperature. The presence of triple bonds on the NP surface was confirmed by adding FAM azide, 5-isomer (Lumiprobe) and visualized by fluorescence microscopy. Both of the resulting algae and NP were washed five times with ultrapure water, removing unreacted NHS ester for the following conjugation. To optimize the binding efficiency, we used different concentrations of NP at 0.04 mg ml^{-1}, 0.2 mg ml^{-1}, and 1 mg ml^{-1} for conjugation. During the conjugation, DBCO-modified NP were incubated with azido-functionalized algae for 45 min. After 3 min centrifugation at 300*g* and three washes

with TAP medium, the resulting algae-NP-robot were collected for further characterization. Static algae-NP were prepared by removing the flagella from the algae using 0.5 M acetic acid, followed by the same procedure for NP conjugation. Cryo-treated algae-NP-robots were prepared by a cryogenic treatment in which the algae-NP-robot was immersed into liquid nitrogen for 45 seconds to maintain the structure of the algae.

Characterization of algae-NP-robot.

To perform scanning electron microscopy (SEM) characterization, algae-NP-robots were first fixed with 2.5% glutaraldehyde overnight at 4 °C and then washed in ultrapure water. After overnight drying, algae-NP-robots were coated with palladium for SEM characterization using an acceleration voltage of 3 KV (Zeiss Sigma 500 SEM instrument). The bare algae and static algae-NP were treated and examined using the same methodology. The attachment of NP to algae was captured by fluorescence microscopy (EVOS FL) with three individual fluorescence channels, Cy5, RFP and GFP, which corresponded to the autofluorescence of algae, the DiI-labeled neutrophil membrane, and the DiO-loaded PLGA cores, respectively.

Algae viability study.

To evaluate algae viability, algae were stained in 5 μM SYTOX green fluorescent probe (Thermo Fisher). The bright green fluorescence of dead algae was examined by fluorescence microscopy. Based on previously reported methods[46], the solution was measured for SYTOX fluorescence intensity ($\lambda_{ex}/\lambda_{em}$ = 504 nm/523 nm) using a plate reader. No washing steps were required due to the specific staining of the nucleic acid of dead algae.

Motion analysis.

The motion of algae-NP-robot and bare algae control was evaluated in simulated lung fluid (SLF). The SLF composition is shown in Supplementary Table 1. The speed of algae-NP-robot in the SLF was measured in the dark at 37 °C, and changes in the motion were evaluated at 1 h, 12 h, 24 h, and 48 h. The speed of algae-NP-robot was also measured over 1 h at an elevated body temperature at 40 °C. The movies of the motion were recorded by optical microscope (Nikon Eclipse Instrument Inc. Ti-S/L 100). An NIS Element tracking module was used to measure the corresponding algae speed in SLF.

Binding of NPs or liposomes with bacteria.

Neutrophil membrane-coated DiO-loaded PLGA nanoparticles (denoted ‘NPs’) and DiO-loaded PLGA nanoparticle cores without membrane coating were prepared as before. Liposomes were synthesized through an extrusion-based method. Briefly, L-α-phosphatidylcholine (EggPC, Avanti Polar Lipids 840051) and cholesterol (Avanti Polar Lipids 700100) were dissolved in chloroform and mixed at a weight ratio of 9:1. To label the liposomes, DiO was dissolved in chloroform and added to the lipid mixture to reach a weight percentage of 2% DiO. The chloroform was evaporated in nitrogen gas. The dried lipid film was hydrated with sterile PBS to reach a total lipid concentration of 5 mg ml^{-1}. The lipid solution was vortexed for 1 min, followed by sonication in a bath sonicator. The re-hydrated lipids were further extruded through a polycarbonate membrane with 100 nm

pore size to form liposomes. To compare the binding effect, 1 mg of NPs, 1 mg PLGA nanoparticle cores without membrane coating and 1 mg of liposomes were incubated with 1 × 10^7 ml^{-1} *P. aeruginosa* overnight, respectively. The unbound NPs, liposomes and PLGA nanoparticle cores without membrane coating were removed through three washing steps by centrifuging at 700g for 2 min. Brightfield and fluorescent images of the three groups were taken on a Life Technologies EVOS FL fluorescence microscope. Fluorescence values from DiO ($\lambda_{ex}/\lambda_{em}$ = 484 nm/501 nm) were quantified using a BioTek Synergy Mx microplate reader. To perform SEM characterization, samples were initially fixed overnight with 2.5% glutaraldehyde at 4 °C, followed by washing with ultrapure water. After overnight drying, samples were coated with palladium for SEM characterization using an acceleration voltage of 3 KV (Zeiss Sigma 500 SEM instrument).

Binding of algae-NP-robot with bacteria.

The PLGA core and neutrophil membrane were labeled with DiO and DiI, respectively. The algae-NP-robot was prepared as before. *P. aeruginosa* was labeled with Hoechst 33342 (Thermo Fisher Scientific) for 30 min at room temperature. The free dye was removed through three washing steps by centrifuging at 3000*g* for 5 min. To explore the binding effect between algae-NP-robot and bacteria, 1 × 10^5 ml^{-1} algae-NP-robot were incubated with 1 × 10^7 ml^{-1} *P. aeruginosa* overnight. The unbound bacteria were removed through five washing steps by centrifuging at 200*g* for 2 min. After fixation in 2.5% glutaraldehyde, brightfield and fluorescent images of the binding between algae-NP-robot and *P. aeruginosa* were taken on a Life Technologies EVOS FL fluorescence microscope. To quantify binding efficiency, 5 × 10^6 ml^{-1} algae-NP-robots were incubated with 5 × 10^6 CFU ml^{-1} *P. aeruginosa* for 1 h. Colonies of total bacterial input and unbound bacteria were counted after 24 h of culture on agar plates.

Cytotoxicity test.

To evaluate cytotoxicity, J774A.1 cells (ATCC TIB-67) and NL20 cells (ATCC CRL-2503) were seeded in 96-well plates at 1× 10^4 cells per well. The cells were then incubated with algae-NP-robot with an algae/ cell ratio of 0.0625, 0.125, 0.25, 0.5, 1.0, 2.0, 4.0, 8.0, 16.0, 32.0, and 64.0 for 24 hours. CellTiter AQueous One Solution cell proliferation assay (Promega) was used to evaluate cell viability, according to the manufacturer's instructions.

Phototaxis of algae-NP-robot.

A small 2 μl droplet of algae-NP-robot was placed on a glass slide without further modification. After 5 s of random motion, the algae-NP-robot sample was illuminated with white light from the top for 30 s. The video was recorded using an optical microscope.

Intratracheal administration.

The intratracheal administration was performed using a modified method based on a previous paper[34]. Specifically, male CD-1 mice (Charles River Labs) were placed under anesthesia with a ketamine (Pfizer) and xylazine (Lloyd Laboratories) cocktail administered at 100 mg/kg and 20 mg kg^{-1}, respectively. To prepare the inoculation, a certain volume of test materials (50 μl algae-NP-robot, static algae-NP, NP, and TAP medium) was injected

into the PTFE feeding tube (cut 6–8 inches in length) by an insulin needle. Then, the feeding tube was inserted 0.5–1.0 cm into the trachea and the inoculum of test materials was administered into the lungs. To avoid escape of the test materials from the lungs, the feeding tube was left in place for 30 seconds.

Ex vivo lung imaging and retention quantification.

All animal experiments were approved by the Institutional Animal Care and Use Committee of the University of California San Diego and performed under the National Institutes of Health (NIH) guidelines. Male CD-1 mice (Charles River Labs) were placed under anesthesia with a ketamine and xylazine cocktail. They were subsequently intratracheally administrated with TAP buffer, 5×10^6 algae-NP-robot, or 5×10^6 static algae-NP. After certain timepoints (1, 4, 12, 24, 48, and 72 h), the mice were euthanized, and their lungs were excised for analysis. Fluorescent *ex vivo* lung images were obtained with the Xenogen IVIS 200 system. Subsequently, the lung samples were homogenized, and fluorescence values were measured on a BioTek Synergy Mx microplate reader. Bacterial dispersion studies were performed with a similar method. Briefly, *P. aeruginosa* bacteria were labeled with DiD after overnight incubation. Following anesthesia, the mice were intratracheally inoculated with 5×10^6 CFU of DiD labeled *P. aeruginosa*. After 1 h inoculation, the mice were euthanized, and their lungs were excised for IVIS imaging analysis.

In vitro macrophage phagocytosis.

J774A.1 macrophage cells were cultured using Dulbecco's modified Eagle medium (DMEM, Invitrogen) in a 24-well plate at density of 1×10^6 cells per well. Algae-NP-robots were then added at a robot/macrophage ratio of 1:1 and incubated at 37 °C. After certain timepoints (1, 4, 12, 24, 48, and 72 h), the mixture was analyzed by fluorescence microscopy and fluorescence values were quantified using a BioTek Synergy Mx microplate reader. Static algae-NP and cryo-treated algae-NP-robot controls were tested and quantified following the same method.

Algae-NP-robot clearance *in vivo*.

At various timepoints (1 h, 4 h, 12 h, and 48 h) before the study, male CD-1 mice were intratracheally inoculated with equivalent amounts of algae-NP-robot or static algae-NP. Then, mice were euthanized by carbon dioxide asphyxiation and the trachea was exposed. A catheter made by tightly fitting a 23-gauge needle into PTFE tubing (Cole Parmer) was inserted into the trachea and secured with sutures. Bronchoalveolar lavage was then collected from each mouse by repeatedly washing the lungs five times with 1 ml of 0.5% (v/v) fetal bovine serum (Gibco) and 2 mM EDTA in PBS and immediately stored on ice. Cells were spun down at 700*g* for 5 min, and red blood cells were lysed using a commercial buffer (Biolegend) following the manufacturer's instructions. Subsequently, nonspecific binding on the cells was blocked with 1% (w/v) BSA in PBS for 15 min and then probed with Pacific Blue conjugated anti-mouse CD11c (N418, Biolegend) and PE-conjugated anti-mouse Siglec-F (S17007L, Biolegend) antibodies for 30 min on ice. Unbound antibodies were washed out twice with 1% BSA in PBS and the cells were resuspended in 1% BSA in PBS for flow cytometry analysis. Data was acquired with a BD FACSCanto II flow cytometer and analyzed using the FlowJo software.

Ciprofloxacin (Cip) loading and release measurement.

A total of 1 ml of algae at different concentrations (1×10^7 ml^{-1}, 2×10^7 ml^{-1}, 4×10^7 ml^{-1}, 8×10^7 ml^{-1}, and 16×10^7 ml^{-1}) was conjugated with 1 mg NP(Cip) by click chemistry, followed by removal of free NP(Cip) by three washes at 300 *g* for 2 min. Then, the algae-NP(Cip)-robots were suspended in 1 ml of TAP for further use. After fabrication of algae-NP(Cip)-robot, the solution was measured for Cip fluorescence intensity ($\lambda_{ex}/\lambda_{em}$ = 270 nm/440 nm). A standard calibration curve was made by measuring serial dilutions of Cip solution (0–10 μg ml^{-1}), and the Cip concentration was determined by comparing with the standard calibration curve. The Cip release was conducted with 1 ml of algae-NP(Cip)-robot at 37 °C within 72 h. Cip concentration was determined also by fluorescence measurement.

In vitro antibacterial activity of algae-NP(Cip)-robot.

A volume of 1 ml of *P. aeruginosa* PAO1 strain (ATCC, BAA-47) at 5×10^6 CFU (colony-forming unit) ml^{-1} was mixed with TAP, free Cip, NP(Cip), static algae-NP(Cip), or algae-NP(Cip)-robot at an equivalent Cip amount. To quantify the minimal inhibitory concentration (MIC) of Cip, various concentrations of Cip were used: 31.25 ng ml^{-1}, 62.5 ng ml^{-1}, 125 ng ml^{-1}, 250 ng ml^{-1}, 500 ng ml^{-1}, and 1 μg ml^{-1}. The bacterial growth was quantified by measuring their absorbance at 600 nm (OD_{600}).

In vivo enumeration study.

P. aeruginosa was first streaked onto a Luria broth (LB; Sigma-Aldrich) agar plate and cultured overnight at 37 °C. A single colony was inoculated in 50 ml of LB, and further cultured for 10 h at 37 °C on shaker. The bacteria were collected after spinning down at 5,000*g* for 20 min, washing with PBS, and resuspending in PBS to a final concentration of 2×10^8 CFU ml^{-1}. Male CD-1 mice were placed under anesthesia with a ketamine and xylazine cocktail. They were intratracheally inoculated with 5×10^6 CFU of *P. aeruginosa* and subsequently intratracheally administered with TAP buffer, NP(Cip), 5×10^6 algae-NP(Cip)-robot, or 5×10^6 static algae-NP(Cip) at an equivalent Cip amount (500 ng). After 24 h, 48 h, 72 h, and 168 h, the mice were euthanized, and their lungs were collected for quantification of bacterial load. In a separate enumeration study, treatment with the algae-NP(Cip)-robot was delayed for 30 min, 2 h, 4 h, and 6 h after the bacterial challenge, and lung samples were collected after another 24 h for enumeration. To compare with the IV treatment, an equivalent Cip amount (500 ng) and a clinical dose (1.64 mg) were intravenous injected separately into mice 30 min after bacterial inoculation. Bacterial enumeration was performed using the same protocol.

In vivo survival study.

Male CD-1 mice were placed under anesthesia using a ketamine and xylazine cocktail. They were intratracheally inoculated with 5×10^6 CFU of *P. aeruginosa* and then intratracheally administered with TAP buffer, NP-Cip, 5×10^6 algae-NP(Cip)-robot, or 5×10^6 static algae-NP(Cip) at an equivalent Cip amount (500 ng). To compare with the IV treatment, an equivalent Cip amount (500 ng) and a clinical dose (1.64 mg) were intravenous injected

separately into mice 30 min after bacterial inoculation. Survival of each mouse was monitored on a daily basis.

In vivo safety studies.

Mice were euthanized at 24 h, 72 h, and 168 h after intratracheal administration of TAP buffer or 5×10^6 algae-NP(Cip)-robot for sample collection. For the comprehensive metabolic panel and blood cell counts, serum and whole blood were collected. Lab tests were carried out by the UC San Diego Animal Care Program Diagnostic Services Laboratory. For histological analysis, H&E staining was performed on major organs. To evaluate the cytokine levels, bronchoalveolar lavage fluid (BALF) was collected by washing the lungs five times using 1 ml of 0.5% (v/v) fetal bovine serum (Gibco) and 2 mM EDTA in PBS through a 23-gauge needle into PTFE tubing (Cole Parmer) inserted into the trachea. For cytokine analysis, the BALF was centrifuged at 700g for 5 min to collect the supernatant. Cytokine concentrations in BALF were measured in triplicate by multiplexed sandwich enzyme-linked immunosorbent assay (ELISA) kit (BioLegend). The histology sections of lung tissue were evaluated by the Tissue Technology Shared Resources, UC San Diego Moores Cancer Center. All histological assessments were performed in a blinded manner to prevent observer bias.

In vitro cytokine production.

J774A.1 macrophage cells were cultured in DMEM in a 6-well plate at 1×10^6 cells per well. They were subsequently incubated with 5×10^6 algae-NP-robot, 5×10^6 cryo-treated algae-NP-robot, 5×10^6 static algae-NP, or 100 ng ml^{-1} flagellin isolated from *Salmonella Typhimurium* bacteria (InvivoGen) for 24 h. Cytokine levels were determined by ELISA kits (BioLegend).

Data availability

The data supporting the findings of this study are available within the paper, its Supplementary Information files and from the corresponding authors upon reasonable request. Source data are provided with this paper.

Supplementary Material

Refer to Web version on PubMed Central for supplementary material.

Acknowledgements

This work is supported by the National Institutes of Health under Award Number R01CA200574 (L.Z.).

References

1. Li J, Esteban-Fernández de Ávila B, Gao W, Zhang L, Wang J Micro/nanorobots for biomedicine: delivery, surgery, sensing, and detoxification. Sci. Robot 2, eaam6431 (2017). [PubMed: 31552379]
2. Gao C et al. Biomedical micro-/nanomotors: from overcoming biological barriers to in vivo imaging. Adv. Mater. 2000512 (2020).
3. Wu Z, Chen Y, Mukasa D, Pak OS, Gao W Medical micro/nanorobots in complex media. Chem. Soc. Rev. 49, 8088–8112 (2020). [PubMed: 32596700]

4. Esteban-Fernández de Ávila B et al. Micromotor-enabled active drug delivery for in vivo treatment of stomach infection. Nat. Commun. 8, 272 (2017). [PubMed: 28814725]
5. Wu Z et al. A microrobotic system guided by photoacoustic computed tomography for targeted navigation in intestines in vivo. Sci. Robot. 4, eaax0613 (2019). [PubMed: 32632399]
6. Wu Z et al. , A swarm of slippery micropropellers penetrates the vitreous body of the eye. Sci. Adv. 4, eaat4388 (2018). [PubMed: 30406201]
7. Gao W et al. , Artificial micromotors in the mouse's stomach: a step toward in vivo use of synthetic motors. ACS Nano 9, 117–123 (2015). [PubMed: 25549040]
8. Wei X et al. Biomimetic micromotor enables active delivery of antigens for oral vaccination. Nano Lett. 19, 1914–1921 (2019). [PubMed: 30724085]
9. Servant A, Qiu F, Mazza M, Kostarelos K, Nelson BJ Controlled in vivo swimming of a swarm of bacteria-like microrobotic flagella. Adv. Mater. 27, 2981 (2015). [PubMed: 25850420]
10. Yan X et al. Multifunctional biohybrid magnetite microrobots for imaging-guided therapy. Sci. Robot 2, eaaq1155 (2017). [PubMed: 33157904]
11. Sun L et al. Biohybrid robotics with living cell actuation. Chem. Soc. Rev. 49, 4043–4069 (2020). [PubMed: 32417875]
12. Ricotti L et al. Biohybrid actuators for robotics: A review of devices actuated by living cells. Sci. Robot 2, eaaq0459 (2017)
13. Felfoul O et al. Magneto-aerotactic bacteria deliver drug-containing nanoliposomes to tumour hypoxic regions. Nat. Nanotechnol. 11, 941–947 (2016). [PubMed: 27525475]
14. Medina-Sánchez M, Schwarz L, Meyer AK, Hebenstreit F, Schmidt OG Cellular cargo delivery: toward assisted fertilization by sperm carrying micromotors. Nano Lett. 16, 555–561 (2015). [PubMed: 26699202]
15. Weibel DB et al. Microoxen: microorganisms to move microscale loads. PNAS 102, 11963 (2005). [PubMed: 16103369]
16. Yasa O, Erkoc P, Alapan Y, Sitti M Microalga-powered microswimmers toward active cargo delivery. Adv. Mater. 30, 1804130 (2018).
17. Silflow CD, Lefebvre PA Assembly and motility of eukaryotic cilia and flagella. Lessons from chlamydomonas reinhardtii. Plant Physiol. 127, 1500–1507 (2001). [PubMed: 11743094]
18. Zhang Q et al. Neutrophil membrane-coated nanoparticles inhibit synovial inflammation and alleviate joint damage in inflammatory arthritis. Nat. Nanotechnol. 13, 1182 (2018). [PubMed: 30177807]
19. Metersky ML, Kalil AC Management of ventilator-associated pneumonia: guidelines. Clin. Chest Med. 39, 797–808 (2018). [PubMed: 30390750]
20. Schreiber MP, Shorr AF Challenges and opportunities in the treatment of ventilator-associated pneumonia. Expert Rev. Anti. Infec. Ther. 15, 23–32 (2017). [PubMed: 27771978]
21. Muscedere J et al. The clinical impact and preventability of ventilator-associated conditions in critically ill patients who are mechanically ventilated. Chest. 144, 1453–1460 (2013). [PubMed: 24030318]
22. Melsen WG et al. Attributable mortality of ventilator-associated pneumonia: a meta-analysis of individual patient data from randomised prevention studies. Lancet Infect. Dis. 13, 665–671 (2013). [PubMed: 23622939]
23. Kharel S, Bist A, Mishra SK Ventilator-associated pneumonia among ICU patients in WHO Southeast Asian region: A systematic review. PloS one 16, e0247832 (2021). [PubMed: 33690663]
24. Vincent J-L, de Souza Barros D, Cianferoni S, Diagnosis, management and prevention of ventilator-associated pneumonia. Drugs. 70, 1927–1944 (2010). [PubMed: 20883051]
25. Kerschgens IP, Gademann K Antibiotic algae by chemical surface engineering. ChemBioChem 19, 439–443 (2018). [PubMed: 29232034]
26. Szponarski M et al. On-cell catalysis by surface engineering of live cells with an artificial metalloenzyme. Commun. Chem. 1, 84 (2018).
27. Shi P et al. Spatiotemporal control of cell–cell reversible interactions using molecular engineering. Nat. Commun. 7, 13088 (2016). [PubMed: 27708265]

28. Wang H et al. Metabolic labeling and targeted modulation of dendritic cells. Nat. Mater. 19, 1244–1252 (2020). [PubMed: 32424368]
29. Hu Q et al. Conjugation of haematopoietic stem cells and platelets decorated with anti-PD-1 antibodies augments anti-leukaemia efficacy. Nat. Biomed. Eng. 2, 831 (2018). [PubMed: 31015615]
30. Fang RH et al. Cell membrane coating nanotechnology. Adv. Mater. 30, 1706759 (2018).
31. Kumar A et al. A biocompatible synthetic lung fluid based on human respiratory tract lining fluid composition. Pharm. Res. 34, 2454–2465 (2017). [PubMed: 28560698]
32. Tanaka Y et al. Acclimation of the photosynthetic machinery to high temperature in chlamydomonas reinhardtii requires synthesis de novo of proteins encoded by the nuclear and chloroplast genomes. Plant. Physiol. 124, 441–449 (2000). [PubMed: 10982457]
33. Singh SP, Singh P Effect of temperature and light on the growth of algae species: a review. Renew. Sust. Energ. Rev. 50, 431–444 (2015).
34. Ortiz-Munoz G, Looney MR Non-invasive intratracheal instillation in Mice. Bio. Protoc. 5, e1504 (2015).
35. Sibille Y, Reynolds HY Macrophages and polymorphonuclear neutrophils in lung defense and injury. Am. Rev. Respir. Dis. 141, 471–501 (1990). [PubMed: 2405761]
36. Justo JA, Danziger LH, Gotfried MH Efficacy of inhaled ciprofloxacin in the management of non-cystic fibrosis bronchiectasis. Ther. Adv. Respir. Dis. 7, 272–287 (2013). [PubMed: 23690368]
37. Oliver A et al. Hypermutation and the Preexistence of Antibiotic-Resistant Pseudomonas aeruginosa Mutants: Implications for Susceptibility Testing and Treatment of Chronic Infections. Antimicrob. Agents Chemother. 48, 4226 (2004). [PubMed: 15504845]
38. Lovewell RR, Patankar YR, Berwin B Mechanisms of phagocytosis and host clearance of Pseudomonas aeruginosa. Am. J. Physiol. Lung Cell. Mol. Physiol. 306, L591–L603 (2014). [PubMed: 24464809]
39. Hayashi F, et al. The innate immune response to bacterial flagellin is mediated by Toll-like receptor 5. Nature 410, 1099 (2001). [PubMed: 11323673]
40. Boyden E et al. Millisecond-timescale, genetically targeted optical control of neural activity. Nat. Neurosci. 8, 1263–1268 (2005). [PubMed: 16116447]
41. Sineshchekov OA, Jung K-H, Spudich JL Two rhodopsins mediate phototaxis to low-and high-intensity light in Chlamydomonas reinhardtii. PNAS 99, 8689–8694 (2002). [PubMed: 12060707]
42. Akolpoglu MB et al. High-Yield Production of Biohybrid Microalgae for On-Demand Cargo Delivery. Adv Sci 7, 2001256 (2020).
43. Delalat B et al. Targeted drug delivery using genetically engineered diatom biosilica. Nat. Commun. 6, 8791 (2015). [PubMed: 26556723]
44. Martel S et al. Flagellated magnetotactic bacteria as controlled MRI-trackable propulsion and steering systems for medical nanorobots operating in the human microvasculature. IJRR 28, 571–582 (2009). [PubMed: 19890435]
45. Zhang Y et al. A bioadhesive nanoparticle–hydrogel hybrid system for localized antimicrobial drug delivery. ACS Appl. Mater. Inter. 8, 18367 (2016).
46. Sato M, Murata Y, Mizusawa M, Iwahashi H, Oka S.-i. A Simple and rapid dual fluorescence viability assay for microalgae. Microbiol. Cult. Coll 20, 53–59 (2004).

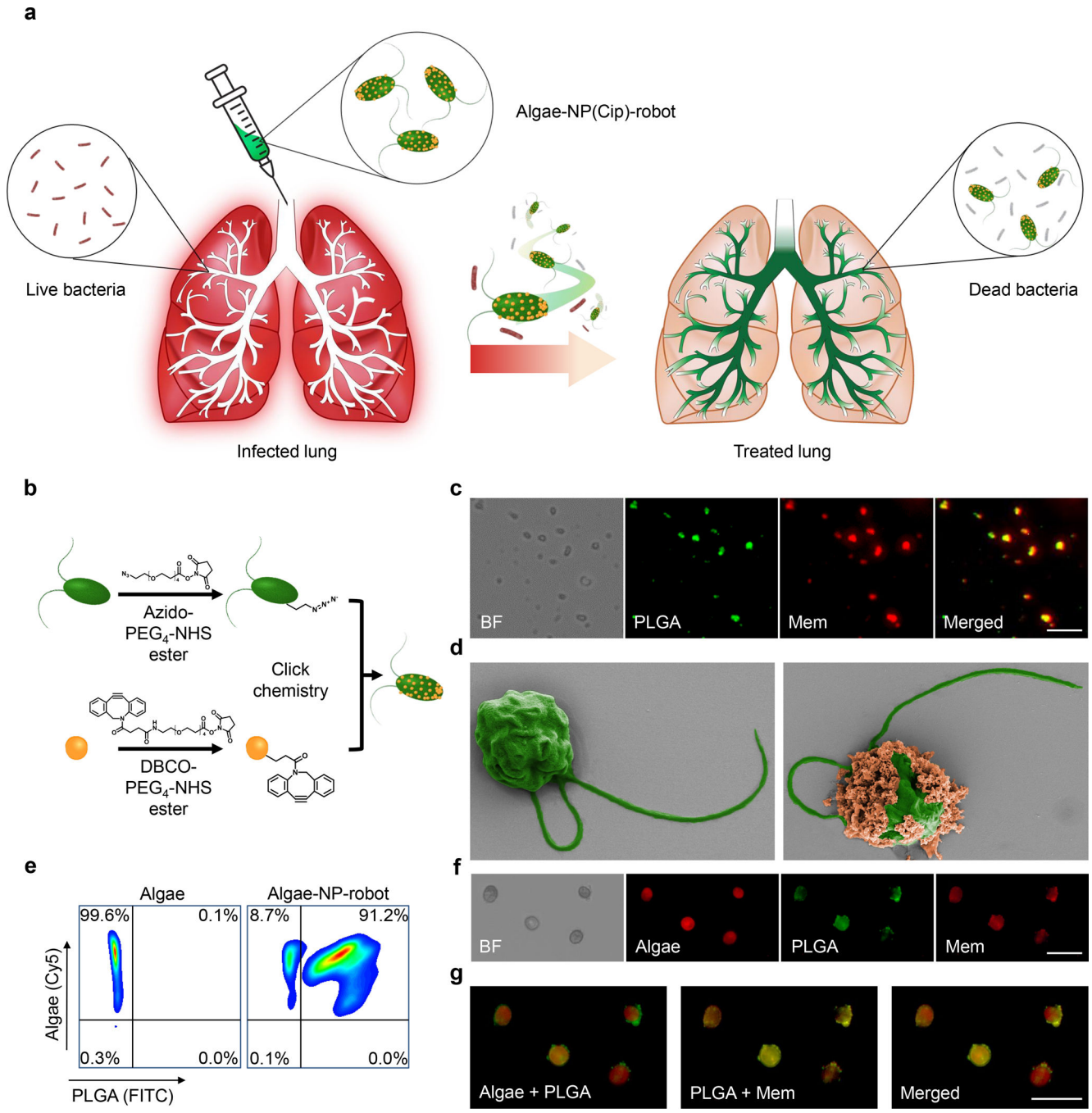

Figure 1 |. Preparation and structural characterization of the algae-nanoparticle hybrid microrobot (denoted "algae-NP-robot").

a, Schematic depicting the use of algae-NP-robot for the treatment of a bacterial lung infection. *C. reinhardtii* algae is modified with drug-loaded NPs and then administered *in vivo* for the treatment of *P. aeruginosa* lung infection. The NP is consisting of neutrophil membrane-coated poly(lactic-*co*-glycolic) (PLGA) core. **b,** Schematic of the functionalization of *C. reinhardtii* with drug-loaded NP using click chemistry. **c,** Brightfield and fluorescent images of the NP, in which the PLGA cores are labeled with DiO (green

color) and the neutrophil membranes are labeled with DiI (red color). Scale bar: 1 μm. **d,** Pseudocolored scanning electron microscopy images of an unmodified algae (left) and an algae-NP-robot (right). Scale bar: 2 μm. **e,** Flow cytometric analysis of algae before (left) and after (right) functionalization with DiO-labeled NP. **f,** Brightfield and fluorescent images of algae-NP-robot. Autofluorescence of natural algae chloroplast in Cy5 channel; DiO-labeled PLGA cores in GFP channel; DiI-labeled cell membranes in RFP channel. Scale bar: 20 μm. **g,** Merged images from (f). Cy5 and GFP channels (left); GFP and RFP channels (center); all three channels (right). Scale bar: 20 μm. In panels c, f, and g, independent experiments were performed (n = 3) with similar results.

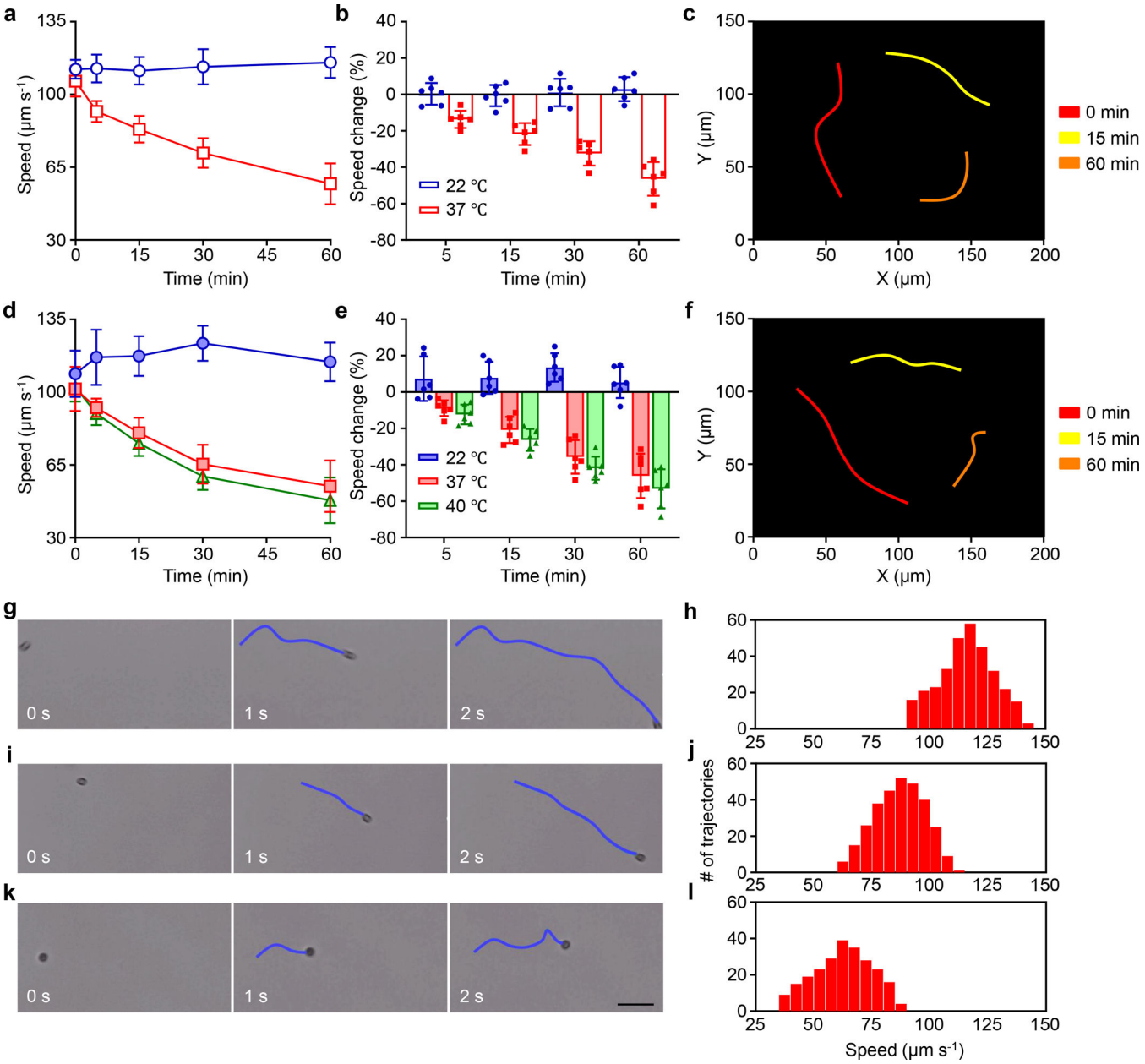

Figure 2 |. Motion behavior of algae-NP-robot.

a-f, Comparison of the speed of bare algae (a,b) and algae-NP-robot (d,e) in simulated lung fluid (SLF) at room (22 °C), body (37 °C), and elevated body (40 °C) temperatures (blue, red, and green bars, respectively) (n = 6; mean ± s.d.). Optical tracking trajectories of the motion of bare algae (c) and algae-NP-robot (f) in SLF at 37 °C over 1 s (obtained at 0, 15, and 60 min: red, yellow, and orange, respectively) (Supplementary Movie 1). **g-l,** Representative trajectories (g, i, and k) from Supplementary Movie 2 corresponding to 0 s, 1 s, and 2 s, respectively, and mean speed distribution (h, j, and l) of algae-NP-robot in SLF at 37 °C after 0 min (g and h), 15 min (i and j), and 60 min (k and l). Scale bar: 50 μm.

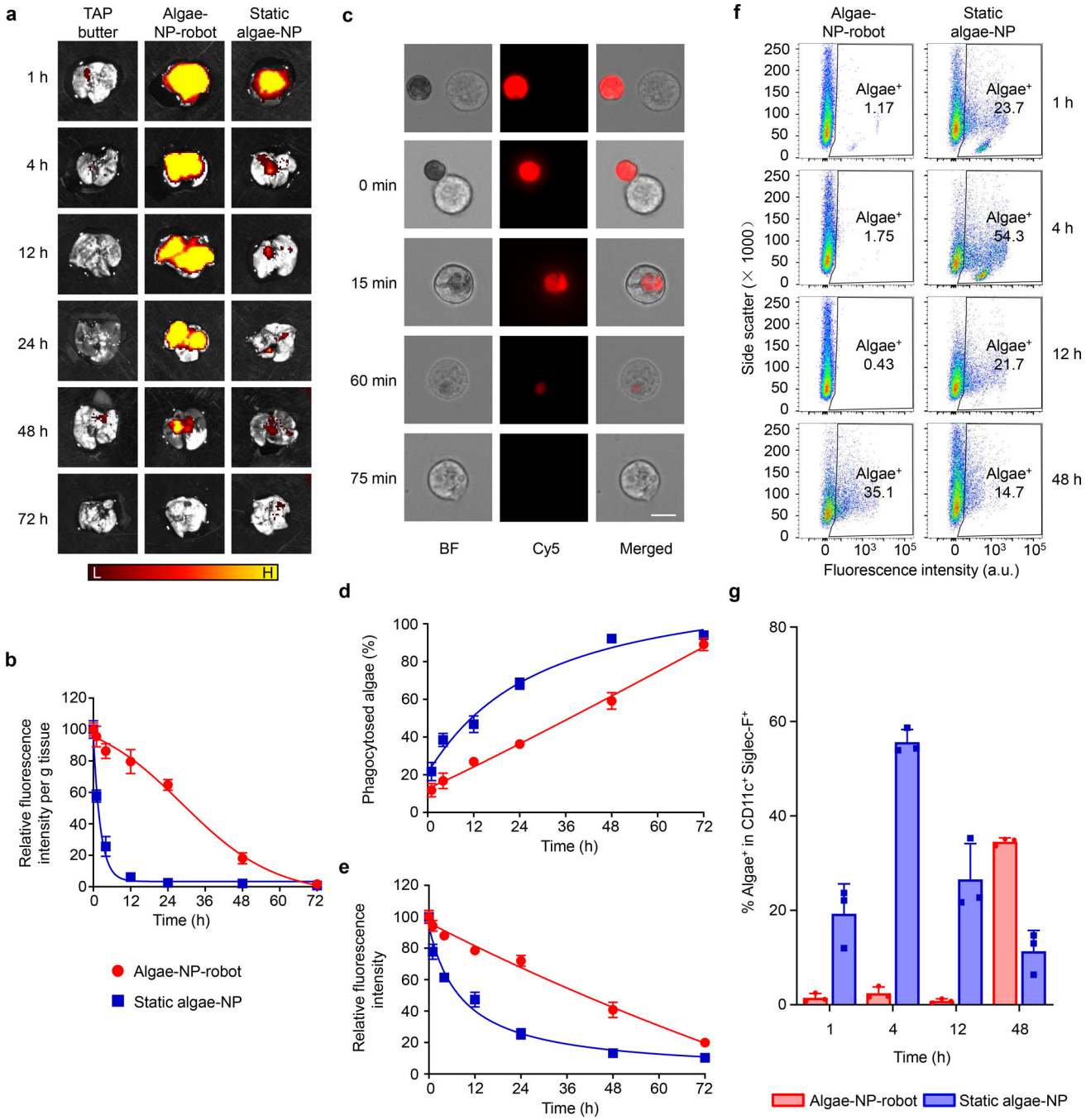

Figure 3 |. Lung distribution of algae-NP-robot.

a, *Ex vivo* fluorescent imaging of lungs at various timepoints after intratracheal administration with tris-acetate-phosphate (TAP) medium, algae-NP-robot, or static algae-NP as a negative control (H, high signal; L, low signal). **b,** Normalized intensity per gram of tissue of lung samples collected in (a) (n = 3; mean + s.d.). **c,** Brightfield and fluorescence microscopy images of representative algae-NP-robot incubated with macrophages at various stages of their interaction. Scale bar = 10 μm. Independent experiments (n = 3) were performed with similar results. **d,** Macrophage phagocytosis of static algae-NP or algae-NP-

robot over time (n = 3; mean + s.d.). **e,** Relative fluorescence intensity of algae-NP-robot or static algae-NP over time after incubation with macrophage cells *in vitro* (n = 3; mean + s.d.). **f**, Representative flow cytometry dot plots of algae-NP-robot (left) and static algae-NP (right) uptake by alveolar macrophages ($CD11c^+$ Siglec-F^+) at various timepoints after intratracheal administration *in vivo*. **g**, Comparison of algae-NP-robot and static algae-NP uptake in alveolar macrophages at various timepoints after intratracheal administration *in vivo* (n = 3; mean + s.d.).

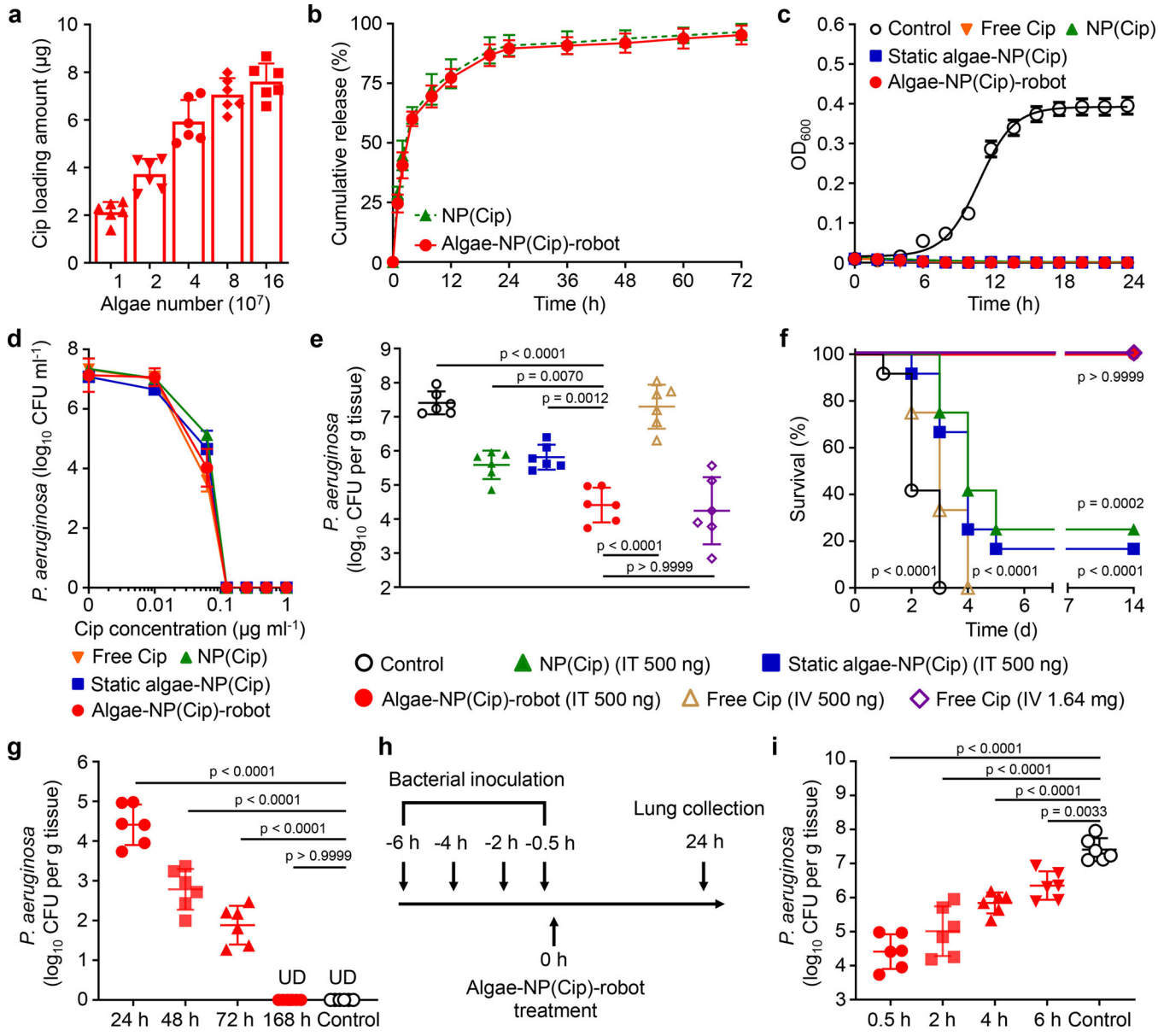

Figure 4 |. *In vivo* therapeutic efficacy of algae-NP-robot.

a, Quantification of ciprofloxacin (Cip) loading on different numbers of algae (n = 6; mean + s.d.). **b**, The cumulative drug release profile of NP(Cip) and algae-NP(Cip)-robot (n = 3; mean + s.d.). **c,** Optical density at 600 nm (OD_{600}) measurements of *P. aeruginosa* treated with control TAP buffer, free Cip, NP(Cip), static algae-NP(Cip), and algae-NP(Cip)-robot (n = 3; mean + s.d.). **d,** *In vitro* antibacterial activity of free Cip, NP(Cip), static algae-NP(Cip), and algae-NP(Cip)-robot against *P. aeruginosa* (n = 3; geometric mean + s.d.). **e,f,** *In vivo* antibacterial efficacy of control TAP buffer, NP(Cip), static algae-NP(Cip), and algae-NP(Cip)-robot with a dosage of 500 ng by intratracheal administration and free Cip with the same dosage of 500 ng as used in intratracheal administration and clinical dosage of 1.64 mg by intravenous (IV) administration in *P. aeruginosa*-infected mice, as determined by bacterial enumeration (e, n = 6; geometric mean +_s.d.) and survival (g, n = 12 per

group) studies. **g.** Quantification of bacterial load in the lungs at 24 h, 48 h, 72 h, and 168 h after the algae-NP(Cip)-robot treatment (n = 6; geometric mean + s.d.). UD: undetectable. **h,i,** Experimental timeline (h) and data (i) for the enumeration of the bacterial load in the lungs of mice treated with algae-NP(Cip)-robot at different times after challenge with *P. aeruginosa* (n = 6; geometric mean + s.d.). one-way ANOVA for **e**, **g**, and **i** and log-rank (Mantel-Cox) test for **f**.

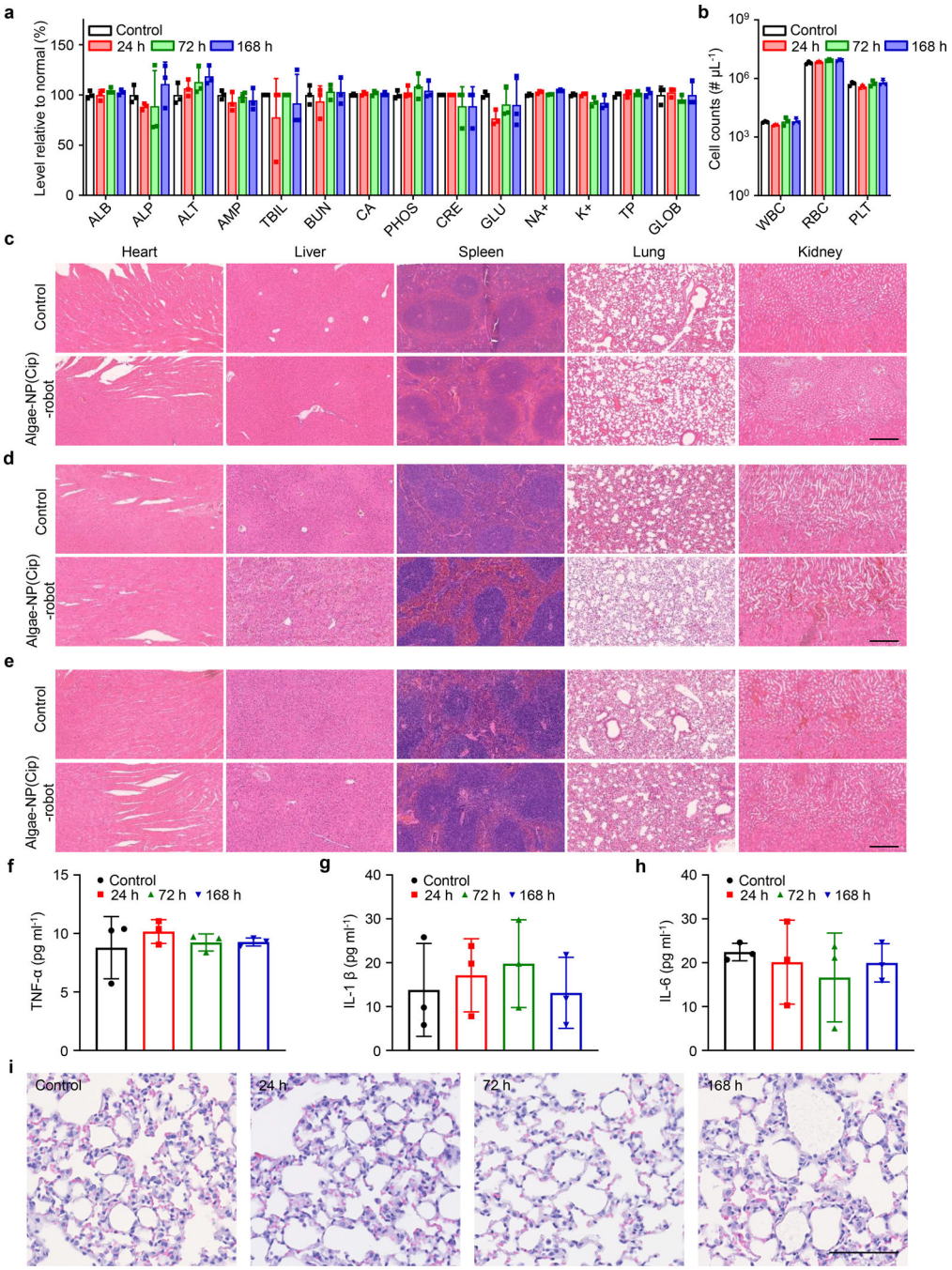

Figure 5 |. *In vivo* safety evaluation of algae-NP(Cip)-robot.

a, Comprehensive blood chemistry panel taken 24 h after intratracheal administration of TAP buffer or 24 h, 72 h, and 168 h after that of algae-NP(Cip)-robot (n = 3; mean + s.d.). ALB: albumin; ALP: alkaline phosphatase; ALT: alanine transaminase; AMY: amylase; TBIL: total bilirubin; BUN: blood urea nitrogen; CA: calcium; PHOS: phosphorus; CRE: creatinine; GLU: glucose; NA^+: sodium; K^+: potassium; TP: total protein; GLOB: globulin. **b,** Counts of various blood cells 24 h after intratracheal administration of TAP buffer or 24 h, 72 h, and 168 h after that of algae-NP(Cip)-robot (n = 3; geometric mean + s.d.). WBC:

white blood cells; RBC: red blood cells; PLT: platelets. **c-e,** Hematoxylin and eosin staining of histology sections from major organs 24 h (c), 72 h (d), and 168 h (e) after intratracheal administration of TAP buffer or algae-NP(Cip)-robot. Scale bar: 250 μm. Independent experiments (n = 3) were performed with similar results. **f-h,** Cytokines, including TNF-α (f), IL-1β (g), IL-6 (h), measured in bronchoalveolar lavage fluid from healthy control mice or 24 h, 72 h, and 168 h after intratracheal administration of algae-NP(Cip)-robot. (n = 3; mean ± s.d.) **i,** Representative images of H&E staining on lung histology sections taken from healthy control mice or 24 h, 72 h, and 168 h after intratracheal administration of algae-NP(Cip)-robot. Scale bar: 100 μm. Independent experiments were performed (n = 3) with similar results.